# Chemically Tunable Electrochemical Dissolution of Noncontinuous Polyelectrolyte Assemblies: An In Situ Study Using ecAFM

**Orane Guillaume-Gentil,* Daniele Abbruzzese, Elsa Thomasson, Janos Vörös, and Tomaso Zambelli**

Laboratory of Biosensors and Bioelectronics, Institute for Biomedical Engineering, ETH and University Zurich, Gloriastrasse 35, 8092 Zurich, Switzerland

**ABSTRACT** The electrochemically triggered dissolution of noncontinuous polyelectrolyte assemblies presenting distinct nanomorphologies and its tuning by chemical cross-linking were monitored locally, in situ, by electrochemical atomic force microscopy. Poly-L-lysine and hyaluronic acid deposited layer-by-layer on indium tin oxide electrodes at specific experimental conditions formed well-defined nanostructures whose morphologies could be easily and precisely followed along the dissolution process. In addition to shrinkage of polyelectrolyte nanodroplets, ecAFM images revealed the faster dissolution of coalesced structures compared to droplet-like complexes, and the readsorption of dissolved polyelectrolytes onto slower dissolving neighboring structures. Covalently cross-linked PLL/HA assemblies dissolved only partially, and exhibited slower dissolution rates compared to native multilayers, with a clear dependence on the cross-link density. Tuning the electrochemical dissolution of polyelectrolyte multilayers through chemical cross-linking opens new prospects for future biomedical applications, such as the development of advanced drug or gene delivery platforms allowing for tightly controlled releases of different compounds at specific rates.

**KEYWORDS:** ITO electrode • polyelectrolyte multilayers • electrochemical dissolution • chemical cross-linking • electrochemical atomic force microscopy

## INTRODUCTION

Simple and versatile, the layer-by-layer assembly of polycations and polyanions is now widely applied for the modification of miscellaneous surfaces in various application fields, including biomedical engineering (1−4). Polyelectrolyte multilayers (PEM) represent unique materials with precisely tunable physical, chemical, and mechanical properties (4, 5). A highly appealing aspect of PEM with regard to biomedical applications is the possibility to incorporate a broad variety of biologically active entities into the polyelectrolyte assemblies. The bioactive components can be either directly embedded into the PEM or first loaded into an incorporable carrier (eg nanoparticles, micelle, dendrimer, cyclodextrin, ...), allowing for the inclusion of a wide range of compounds including peptides, proteins, enzymes, drugs, or nucleic acids. PEM provide a protective environment to the bioactive moieties, preserve their functionality, and allow for a fine control over their localization and amount (3, 4). The great potential of PEM as reservoir for drugs fostered their use for controlled release platforms (6−9). PEM are most notably used as films or microcapsules that can release bioactive components passively or in response to environmental stimuli, through controlled permeability or degradation of the assembly. Alternatively, the use of external stimuli allows for triggering drug release on demand, irrespective of the environmental conditions. Various external stimuli have been used, such as magnetic field (10, 11), ultrasound (12, 13), electrochemical (14−18), or light (19−21). Among them, the electrochemical trigger is particularly appealing because it enables a precise control over the dissolution process, while presenting valuable advantages such as low costs and the possibilities for automation, miniaturization, patterning and remote control. In addition, electrochemical stimuli are fast, reversible, and local, allowing for sustained or pulsatile release and for application in physiologically relevant environments, without affecting the bulk solution. Previous works have reported the controlled release upon PEM electrochemical dissolution of heparin (15, 22) or nucleic acids (16−18, 23) used as polyanionic components or dextran sulfate (14) conjugated with a polycationic carrier. Beside these studies demonstrating its great potential for drug/gene delivery, the electrochemically stimulated dissolution of LbL assemblies has also been applied for biosensing (24) and cell sheet engineering (25).

For all these applications, the design of reliable, tightly controlled electrochemically addressable platforms requires a deep understanding of the dissolution process. Recent studies on the dissolution of polyelectrolyte assemblies from indium tin oxide (ITO) electrodes upon application of small oxidative voltages evidenced a dissolution mechanism based on the continuous production of protons at the electrode surface through water electrolysis (15, 26). While the protons diffuse from the working electrode, hydroxide are simultaneously produced and diffusing from the counter electrode,

* To whom correspondence should be addressed. Phone: +41 44 632 31 25. Fax: +41 44 632 11 93. E-mail: guillaume@biomed.ee.ethz.ch.

Received for review August 7, 2010 and accepted October 26, 2010

DOI: 10.1021/am1007062

leading to the establishment of a stable pH gradient between the two electrodes, whose extent and strength directly depend on the current density/voltage applied and the buffer concentration in the cover medium (27). The resultant pH decrease in the vicinity of the ITO electrode induces the dissolution of the polyelectrolyte assemblies through neutralization of the negative charges on the polyanion chains and on the surface, while counter-anions migrate from the bulk solution to compensate for the excess of positive charges on the polycation chains.

In a first part, the present work intends to further understand the dissolution process of PEM. The electrochemically induced dissolution of layer-by-layer assemblies of poly L-lysine (PLL) and hyaluronic acid (HA) was monitored in situ using electrochemical atomic force microscopy (ecAFM). While the previous works assessed the dissolution on continuous polyelectrolyte thin films, this study focuses on discontinuous assemblies, allowing for more detailed observations of nanomorphological changes under the electrochemical stimulus. The local observations showed that morphologically, the dissolution followed reversely the growth process, with a heterogeneous dissolution of assemblies presenting coalesced structures and nanodroplets. Non continuous polyelectrolyte assemblies presenting specific, distinct nanomorphologies are formed in particular with weak polyelectrolytes, such as PLL and HA, at the initial phase of the multilayer growth. The deposition of one bilayer of weak polyelectrolytes generally leads to the formation of complexes (nanodroplets), which grow and coalesce upon the deposition of additional bilayers, finally covering the whole surface (28, 29). In most cases, continuous thin films are reached after the deposition of a few bilayers, and with further deposition cycles, the film can reach up to several micrometers in thickness. However, as the formation of weak polyelectrolyte multilayers is highly sensitive to the build-up conditions (polyelectrolytes, substrate, and buffer properties), this initial noncontinuous surface coverage featuring separated polyelectrolyte islands can also last over a relatively high number of deposition cycles, as shown in this study.

While understanding the dissolution process is crucial to enable the design of efficient release systems, means to tailor the dissolution process are desired to achieve optimal release rates. In previous works, the dissolution of PEM has been shown adjustable by the amplitude of the applied electrochemical stimulus (18, 22, 30), the buffer concentration in the bulk solution (27), or the polyelectrolyte components used (15, 26). In the second part of this paper, a novel approach for tuning PEM dissolution is presented, using chemical cross-linking. PLL/HA assemblies hold together mainly through electrostatic interactions between amino groups on PLL chains and carboxylate groups on HA chains. The reaction of these groups with a water-soluble carbodiimide, *N*-(3-Dimethylaminopropyl)-*N*′-ethyl-carbodiimide (EDC), allows for the transformation of electrostatic into covalent cross-links within the multilayer, with such cross-linking reaction favored in the presence of *N*-hydroxysulfosuccinimide (s-NHS) (31−33). This cross-linking method can be applied to any polyelectrolyte system presenting primary amine and carboxylic groups (34). The formation of covalent bonds within polyelectrolyte multilayers has been shown to substantially increase their Young's modulus (35, 36), leading typically to strong improvement of their cell adhesive properties (35, 37−40). Indeed, typical polyelectrolyte systems presenting amine and carboxylic groups are natural polypeptides and polysaccharides, which represent excellent candidates for biomedical applications in term of biocompatibility, but assemble however into soft and highly hydrated PEM with poor cell adhesive properties. The stiffening of these PEMs through cross-linking with EDC/s-NHS dramatically improved their cell adhesive properties, while maintaining their biocompatibility. In addition, a fine-tuning of the cross-link density could be achieved through variations in the cross-linker concentration (36), allowing to generate, with the same polyelectrolyte system, a broad panel of substrates with specific elastic and cell adhesive properties. Parallely, cross-linking also helps stabilizing the PEM. While cross-linking has been proven to improve the resistance of weak polyelectrolyte assemblies against degradation by solvents, pH, ionic strength, or enzymes (32, 41), we studied in the present work the partial stabilization of PLL/HA assemblies against electrochemical dissolution, aiming at the development of smart electrochemically responsive platforms with tunable release rate for controlled drug/gene delivery applications.

## EXPERIMENTAL SECTION

**Polyelectrolytes and Solutions.** Poly-L-lysine hydrobromide (PLL, $M_w$ ∼15−30 kDa) and hyaluronic acid sodium salt from bovine vitreous humor (HA, $M_w$ ∼300 kDa) were obtained from Sigma Aldrich (Switzerland) and used at a concentration of 0.5 mg/mL in buffer solution. The buffer solution was 10 mM 4-(2-hydroxyethyl)-1-piperazine ethanesulfonic acid (HEPES, Fluka, Switzerland) with 150 mM NaCl, pH adjusted to 7.4 with NaOH (HEPES-2).

**Preparation of $(PLL/HA)_n$ Coatings.** Indium tin oxide (ITO) coated glass substrates (Microvacuum, Hungary) were cleaned by 10 min ultrasonication in isopropanol, 10 min ultrasonication in Millipore water, $N_2$-blow drying, and 2 min $O_2$ plasma treatment. The PLL/HA multilayers were built on the substrates by dip and rinse process, with adsorption step of 5 min followed by rinsing step in HEPES-2 for 2 min.

**Cross-Linking Procedure.** *N*-Hydroxysulfosuccinimide sodium salt (s-NHS) and *N*-(3-dimethylaminopropyl)-*N*′-ethylcarbodiimide hydrochloride (EDC) were purchased from Sigma Aldrich (Switzerland) and used at final concentrations of respectively 40 mM and 10 mM (40/10) or 400 mM and 100 mM (400/100) in HEPES-2 buffer. $(PLL/HA)_6$-coated ITO electrodes were incubated overnight at 4 °C in the EDC/s-NHS solution, and rinsed 5 times with HEPES-2.

**Electrochemical Atomic Force Microscopy (ecAFM).** We used the Nanowizard I BioAFM (JPK Instruments, Germany) and the Mikromasch CSC38/noAl cantilevers both in contact and intermittent-contact modes. To observe the morphology of the film in situ, we conceived a Teflon electrochemical liquid-cell provided with a three electrode configuration system, with a silver wire acting as Ag/AgCl reference electrode, a platinum wire as counter electrode, and the ITO surface of the substrate contacted with a metallic copper spring as working electrode. Electrochemical dissolution was achieved through the applica-

tion of an external potential of +1.9 V or a current density of +30 $\mu$A/cm$^2$, using an AMEL potentiostat/galvanostat (model 2053, AMEL electrochemistry, Italy). No buffer flow has been applied during the electrochemical treatment.

**Data Analysis.** ecAFM height mode images were further processed using SPM image processing software (JPK Instruments, Germany). Processed images were exported as ASCII files for further calculation in MatLab. As AFM output data is pixilated the most accurate way to calculate the volume was to multiply each pixel value with its area to create one pixel volume. The pixel volumes were then added together to represent the entire volume of the PEM structures.

## RESULTS

**Formation of Noncontinuous PLL/HA Assemblies.** In our working conditions, the deposition of up to 24 bilayers of PLL/HA onto ITO electrodes yielded noncontinuous coatings, as shown by AFM images (Figures 1A–D and S1). When the first PLL/HA bilayer was deposited, the polyelectrolytes formed nanocomplexes randomly distributed on the surface, covering less than 1 % of the substrate, with heights ranging from 5 to 20 nm (Figure 1A). By increasing the number of deposited bilayers, the density of the nanodroplets on the surface first increased (Figure 1B), and successive deposition cycles led to coalescence and further growth yielding bigger, heterogeneous nanostructures (Figure 1C and D). While the nanostructures reached up to several hundreds of nanometers in height with 15, 18, or 24 deposited bilayers (Figure S1), the coverage of the surface remained incomplete, as confirmed by scratches in the coatings (Figure S2). The volume of adsorbed polyelectrolytes on the electrode increased exponentially with the number of deposited bilayers, as calculated from AFM images (Figure 1E).

**Electrochemical Dissolution.** As previously reported (25, 26), PLL/HA multilayers assembled on ITO electrodes can be dissolved upon the application of small voltages. In this study, the electrochemically induced dissolution of noncontinuous PLL/HA assemblies was monitored in situ by ecAFM under the application of an external potential of +1.9 V, following morphological changes at the nanoscale. In general, ecAFM images of the PLL/HA nanostructures showed the gradual and fast dissolution of all the coatings assessed. Individual nanodroplets shrinked evenly and rapidly upon electrochemical treatment, as shown in Figure 2 with the dissolution of a $(PLL/HA)_3$ coating. Larger coalesced islands also smoothly dissolved during the electrochemical treatment, sometimes splitting back into several nanostructures. (Figure 3) This phenomena became more evident in the case of heterogeneous coatings with bigger coalesced structures, such as $(PLL/HA)_{12}$ assemblies: at first, the large coalesced structures dissolved, revealing underlying droplets that dissolved afterward. (Figure 4) Interestingly, while the large coalesced structures dissolved, some smaller underlying or neighboring nanostructures gained in size before their subsequent dissolution (Figure 4).

**Tuning the Dissolution by Chemical Cross-Linking.** The electrochemically induced dissolution of PLL/HA assemblies was further assessed on chemically cross-linked coatings. The cross-linking reaction between PLL/HA multilayers and a water-soluble carbodiimide, EDC, in combination with sulfo-NHS, leads to the formation of covalent amide bonds between primary amines of PLL and carboxylate groups of HA, and the degree of cross-linking can be tuned by varying the cross-linker concentration (31–33, 36). The dissolution of native $(PLL/HA)_6$ multilayers was thus compared to those of assemblies cross-linked using either 40 mM EDC in combination with 10 mM sulfo-NHS, or 400 mM EDC with 100 mM sulfo-NHS. As the dissolution process relies on the production of protons at the electrode upon electrochemical treatment which is directly proportional to the

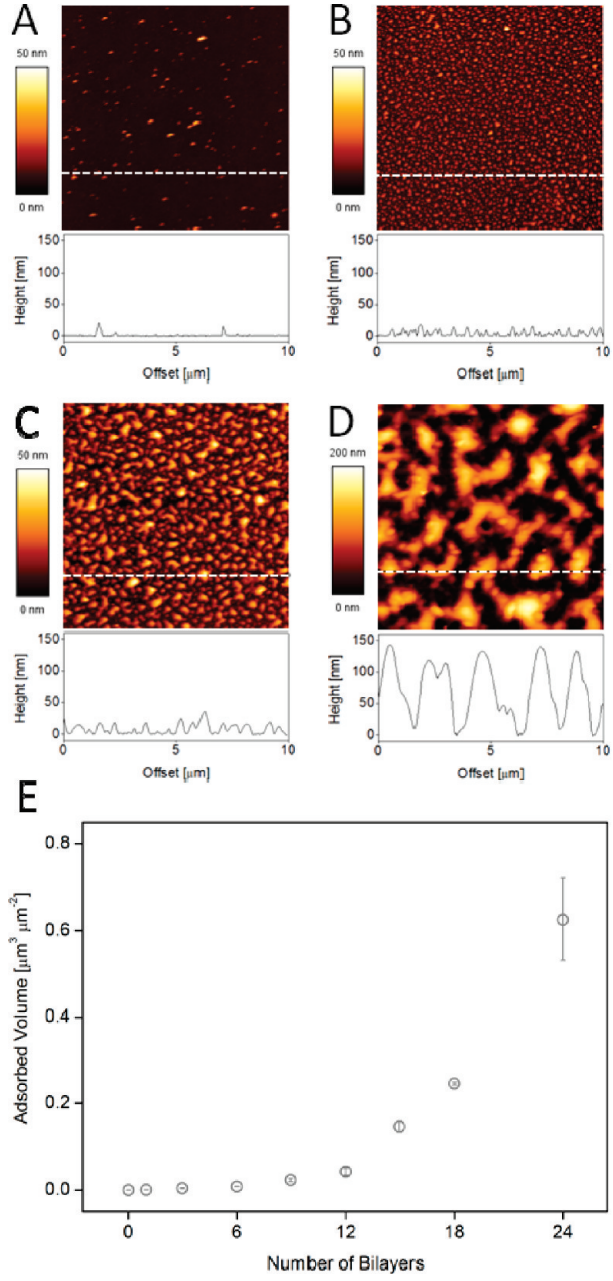


**FIGURE 1. (A–D) 10 × 10 $\mu$m$^2$ AFM height mode images of 1 (A), 3 (B), 6 (C), and 12 (D) bilayers of PLL/HA deposited on ITO electrodes. The profile under each image corresponds to the white line. (E) Volume of PLL/HA adsorbed on the ITO electrodes as a function of the number of deposited bilayers. Error bars are standard errors of the mean of 3–5 measurements.**

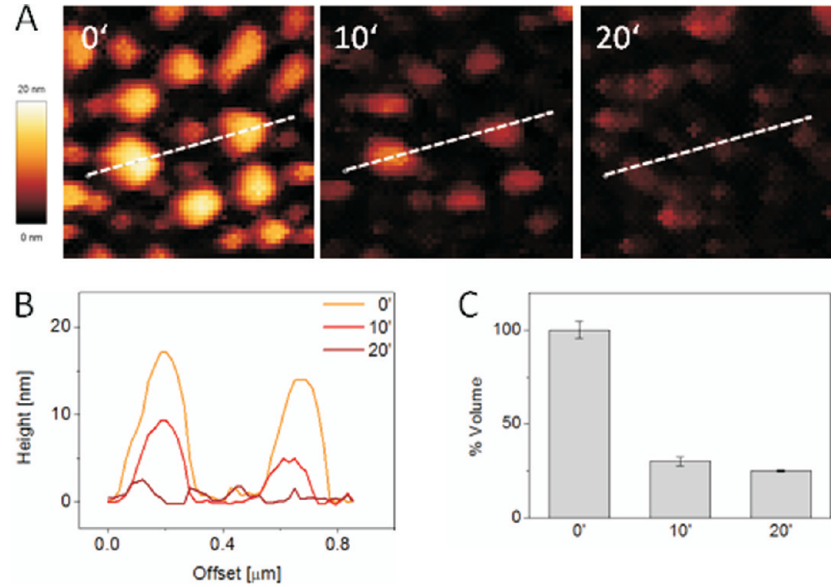


FIGURE 2. Shrinkage of nanodroplets. Dissolution at 1.9 V of $(PLL/HA)_3$ as followed by ecAFM, with (A) $1 \times 1\ \mu m^2$ height mode images of the assembly initially and after 10 and 20 min of electrochemical treatment, (B) the profiles corresponding to the white dashed lines in the AFM height mode images, and (C) the calculated volumes of polyelectrolyte adsorbed on the electrode at the different time points of dissolution. The volumes were calculated from $2.5 \times 2.5\ \mu m^2$ height mode images, and the error bars are standard errors of the mean of 3 measurements.

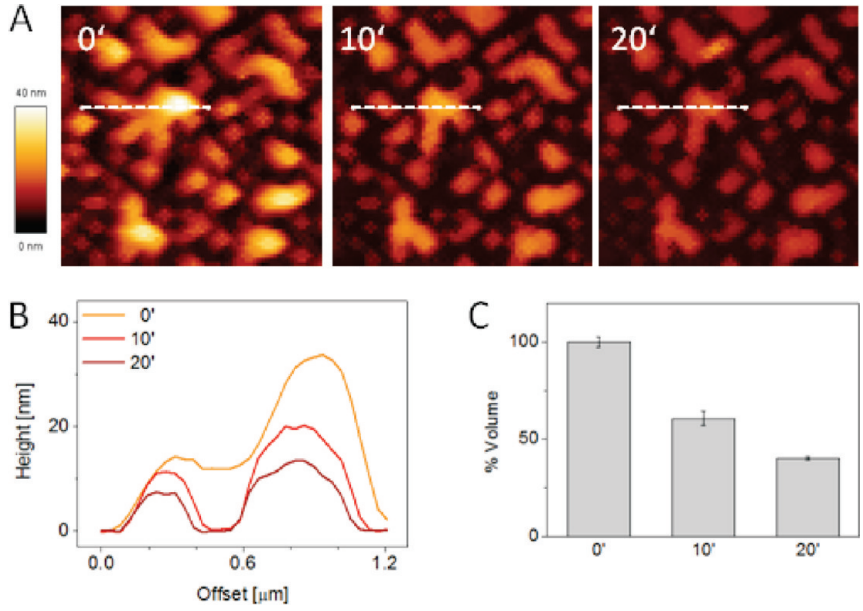


FIGURE 3. Small coalesced islands splitting back into several nanostructures. Dissolution of $(PLL/HA)_6$ islands at +1.9 V as followed by ecAFM. Panel A shows $2.5 \times 2.5\ \mu m^2$ height mode images initially and after 10 and 20 min at +1.9 V. Panel B shows the profiles corresponding to the white dashed lines on the images. Panel C shows the calculated volumes of adsorbed polyelectrolytes during the dissolution, averaged from 3 measurements. Error bars are standard errors of the means.

current density (15, 26, 27), the following experiments were performed in galvanostatic mode allowing for a direct comparison of the samples. A constant current density of $+30\ \mu A\ cm^{-2}$ was then applied, corresponding to potentials of $+1.9 \pm 0.2$ V.

While it did not dramatically affect the initial morphologies of the $(PLL/HA)_6$ coatings (Figure S3), the chemical cross-linking significantly influenced the dissolution process, affecting both the dissoluble fraction and the dissolution rate of the polyelectrolyte assembly. (Figures 5 and S3) The native coating dissolved nearly completely within 120 min, with less than 1 % of the initial volume remaining at the end of the electrochemical treatment. Contrastingly, the cross-linked coatings dissolved only partially, with more than 30 and 50 % residual volumes for 40/10 and 400/100 mM EDC/s-NHS respectively. All the dissolution curves stabilized after about 120 min of electrochemical treatment. Fitting of the dissolution curves with exponential decays (15, 18) gave approximated dissolution constants of 33, 37, and 42 min for 0/0, 40/10 and 400/100 mM EDC/s-NHS respectively, evidencing a slower dissolution for a higher concentration of cross-linking agents. ($R^2$ = 0.999, 0.966, and 0.974, respectively.)

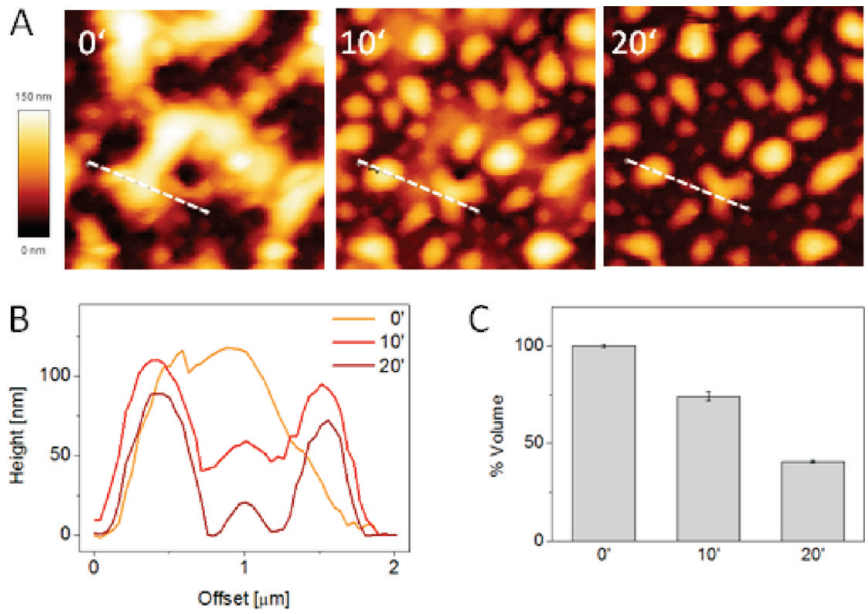


**FIGURE 4. Heterogeneous dissolution of large coalesced structures. Dissolution of $(PLL/HA)_{12}$ at 1.9 V with (A) $5 \times 5\ \mu m^2$ height mode images initially and after 10 and 20 min at +1.9 V, (B) profiles corresponding to the white dashed lines, and (C) calculated volumes of adsorbed polyelectrolytes. Volumes are the mean of 3 measurements with standard errors of the mean as error bars. The large coalesced structures dissolved at first while a size increment was observed for underlying and neighboring smaller structures prior to their dissolution.**

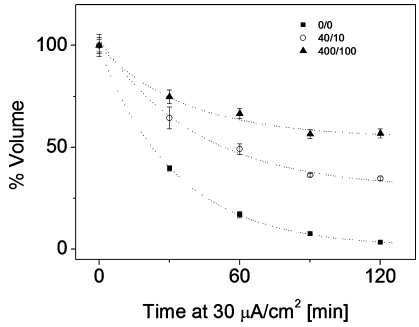


**FIGURE 5. Tuning of the electrochemical dissolution by chemical cross-linking. The dissolution of native (filled squares), or cross-linked $(PLL/HA)_6$ assemblies (40 mM EDC/10 mM s-NHS (empty circles) and 400 mM EDC/100 mM s-NHS (filled triangles)) is represented as the percentage of initial volume as a function of the time under the electrochemical stimulus (+30 $\mu A/cm^2$). The volumes, calculated from AFM height mode images, are the mean of 4 measurements and the error bars are standard error of mean. The dashed lines are exponential decay fittings.**

## DISCUSSION

Combined with in situ ecAFM technique, noncontinuous PLL/HA assemblies presenting distinct nanostructures enabled perceptive observations, locally, of a dynamic dissolution process, evidencing nanoscaled morphological changes of the polyelectrolyte assemblies under electrochemical stimulus. Formation of such specific nanoarchitectures during the initial phase of polyelectrolyte multilayers growth has been reported earlier, the build-up beginning with the formation of nanometer-sized droplets, which coalesce and grow during the first few deposition cycles and ultimately form continuous films (28, 42). This growth scheme is highly dependent on the experimental conditions, the multilayers' internal structure being strongly influenced by a variety of factors, such as the polyelectrolyte used, their molecular weight (43), their concentration (44), the deposition time (44), underlying substrate (42, 45, 46), pH (47–49), ionic strength (50, 51), or the temperature (52), and weak polyelectrolytes multilayers such as PLL/HA are particularly sensitive. In our specific working conditions, up to 24 bilayers of PLL/HA could be deposited while remaining in this early growth phase presenting discontinuous nanoarchitectures. The volume of adsorbed polyelectrolytes increased with the number of deposited bilayers, similarly to the exponentially growing multilayers. It has to be noted that whereas such noncontinuous coatings are particularly well suited for ecAFM investigations, their heterogeneity severely complicates their characterization by means of conventional techniques such as quartz crystal microbalance (53) or optical waveguide lightmode spectroscopy (54, 55), requiring particular modeling for inhomogeneous layers (56–59).

As we recently reported (26), PLL/HA thin films assembled on ITO electrodes readily dissolve upon application of small positive voltages. The dissolution process is induced by the generation of protons upon water electrolysis at the electrode surface, leading to the neutralization of negative charges on HA chains and consequent extrinsic compensation of the resulting excess of positive charges on PLL chains by counter-anions. The weakening of the electrostatic interactions holding the PLL/HA assembly together allows for the diffusion and release of neutralized polyelectrolyte chains into the bulk solution, hence the dissolution of the multilayer. As expected, the non continuous PLL/HA coatings dissolved likewise upon electrochemical treatment. While nanodroplets simply shrinked gradually until complete dissolution, the dissolution of coalesced structures unravelled interesting phenomena. Apparently following the reverse order of the build-up, the dissolution of coalesced nanostructures preceded the nanodroplets shrinkage. While rapidly fading away, the coalesced structures often melted into several structures or unveiled underlying nanodroplets. These ob-

servations intuitively indicate that the coalesced islands are less dense than the nanodroplets structures, hence their faster dissolution. Also, the unraveling of droplets underlying the coalesced structures upon dissolution suggests that the specific nanoarchitectures observed during build-up at each deposition cycle remain stable, without structural rearrangements, upon the successive layer adsorptions. Of interest as well, the initial size increment observed for nanodroplets or small structures underlying or adjacent to the dissolving coalesced islands evidenced a partial readsorption of dissolved polyelectrolyte chains on these neighboring structures. Since local, this phenomenon is assessable only by in situ AFM. As this initial size increase was not observed by the dissolution of coatings presenting individual droplets, an eventual swelling of the droplets before dissolution has to be excluded, and the gained volume can be attributed to material readsorption. However, readsorption from solution is an unlikely process therefore we postulate another hypothesis that can explain this observation: The "free" space in between the droplets is likely to be covered by a monolayer of the polymer that was deposited last, that is, HA. Upon application of electrochemical current this layer rapidly desorbs from the surface and HA molecules from the droplets diffuse onto the free surface. The driving force behind this process is the repulsion within the droplet because of its negative Donnan potential and the interaction with the surface. These new molecules are then also subject to electrochemical removal and the process continues inducing the bottom-up dissolution of the droplets.

As described above, the dissolution process relies on the neutralization of electrostatic interactions within the polyelectrolyte assembly. The replacement of electrostatic interactions within the assembly by covalent bonds is thus expected to affect the dissolution process. PLL/HA multilayers were chemically cross-linked with EDC, a water-soluble carbodiimide, in combination with s-NHS, to induce the formation of covalent amide bonds between the amine groups of PLL and the carboxylate groups of HA (32). While preserving the biocompatibility of PLL/HA assemblies, this cross-linking method allows for tailoring the cross-linking degree of the assembly through variations in reaction time or cross-linker concentration (32, 35, 37). In this study, the electrochemically induced dissolution of native versus cross-linked $(PLL/HA)_6$ assemblies was compared, using two different concentrations of cross-linking agents. The results showed a substantial modulation of the dissolution, with a clear dependence on the EDC/s-NHS concentration. While native assemblies entirely dissolved within 2 h of electrochemical treatment, the cross-linked ones dissolved only partially, with more than 30 and 50% residual volumes for 40/10 and 400/100 mM EDC/s-NHS, respectively. The amount of residual material after dissolution probably correlates with the amount of amide bonds formed within each assembly, with the non cross-linked polyelectrolyte chains neutralized and released during electrochemical treatment while covalent bonds formed within the assembly, unsensitive to the electrochemical stimulus, hold the remaining polyelectrolyte chains together. Interestingly, varying the cross-linking degree of the PLL/HA assemblies resulted not only in different dissoluble amounts, but also in different dissolution rates. Indeed, the dissolution curves showed cross-link density-dependent dissolution rates, with all the dissolution curves stabilizing after about 120 min at 30 $\mu A/cm^2$, while the amount of dissolved polyelectrolytes decreased with increasing cross-linking density.

Finally, while the higher cross-linker concentration used in this study evidently impaired the dissolution, the coating still partially dissolved, indicating an incomplete cross-linking. Boudou et al. reported that a presumably complete cross-linking of PLL/HA assemblies was obtained in their experimental conditions with 800 mM EDC, which resulted in the consumption of ~90% of the carboxylate groups in the assembly, the remaining 10% not being involved in electrostatic interactions with amino groups but associated with counterions (34). With 400 mM EDC, the consumption was reduced to 80%. Using similar experimental conditions, Ren et al. obtained a lower cross-linking degree, with ~65% carboxylate groups consumed with 400 mM EDC (39). In this work, the cross-linking degree obtained with 400 mM was apparently lower, as only ~55% of the assemblies remained undissolved. This low cross-linking efficiency is most probably related to the fact that the cross-linking reactions were performed in solutions buffered at pH 7.4, while in the cited references slightly acidic pHs (5.0–5.5) in which the cross-linking reaction is favored were used. A higher cross-link density completely inhibiting the assembly dissolution could probably be achieved by further increasing the cross-linker concentration, using longer reaction time, or performing the cross-linking reaction at a more favorable pH.

## CONCLUSIONS

The electrochemically induced dissolution of non continuous PLL/HA nanostructures was monitored in situ by ecAFM, revealing morphological details of the dissolution process. Confirming the proton-based dissolution mechanism reported earlier (26), the partial replacement of sensitive electrostatic interactions by covalent bonds allowed for tuning the electrochemical dissolution on a cross-link density dependent fashion. The electrochemical dissolution of polyelectrolyte assemblies, offering precise control over the release of the assembly components and the possibilities for automation, miniaturization, remote control, and micropatterning, has already shown great promises for biomedical applications such as controlled drug (14, 15, 22, 60, 61) and gene (16–18, 62) release, cell sheet engineering (25), or biosensing (24). The controlled modulation of the dissolution process by chemical cross-linking demonstrated in this study offers further new perspectives. The design of compartimented polyelectrolyte architectures with distinct cross-link densities would enable the simultaneous release of several compounds at different rates. Electrochemically responsive PLL/HA platforms have also been applied for the release of intact cell sheets for tissue engineering applications. Despite the good biocompatibility of PLL and HA, the relatively poor cell adhesive properties of PLL/HA assemblies represent the

main limiting factor of this approach. A mild cross-linking would dramatically improved cell adhesive properties (37), while still allowing for partial dissolution of the sacrificial cell substrate as required for cell sheet release.

**Acknowledgment.** The authors thank Stephen Wheeler for his technical assistance and Fouzia Boulmedais for fruitful discussions. The Competence Centre for Material Science and Technology (CCMX) and the Germaine-de-Staël program for Franco-Swiss collaborations are acknowledged for financial support.

**Supporting Information Available:** Morphology of $(PLL/HA)_n$ coatings, $n = 1$ to 24, as observed by AFM (Figure S1), AFM height mode images of scratched $(PLL/HA)_n$, with $n =$ 12, 18, and 24, showing the noncontinuous surface coverage (Figure S2), and ecAFM height mode images of the dissolution at 30 $\mu$A cm$^{-2}$ of $(PLL/HA)_6$ assemblies, native or cross-linked with 40/10 or 400/100 mM/mM EDC/s-NHS (Figure S3). This information is available free of charge via the Internet at http://pubs.acs.org.

## REFERENCES AND NOTES

(1) Katsuhiko, A.; Hill, J. P.; Lee, M. V.; Vinu, A.; Charvet, R.; Acharya, S. *Sci. Technol. Adv. Mater.* **2008**, *9*, 014109.
(2) Wang, Y.; Angelatos, A. S.; Caruso, F. *Chem. Mater.* **2007**, *20*, 848–858.
(3) Tang, Z.; Wang, Y.; Podsiadlo, P.; Kotov, N. A. *Adv. Mater. (Weinheim, Ger.)* **2006**, *18*, 3203–3224.
(4) Boudou, T.; Crouzier, T.; Ren, K.; Blin, G.; Picart, C. *Adv. Mater. (Weinheim, Ger.)* **2010**, *22*, 441–467.
(5) Ariga, K.; Hill, J. P.; Ji, Q. *Phys. Chem. Chem. Phys.* **2007**, *9*, 2319–2340.
(6) De Geest, B. G.; Sanders, N. N.; Sukhorukov, G. B.; Demeester, J.; De Smedt, S. C. *Chem. Soc. Rev.* **2007**, *36*, 636–649.
(7) Jiang, B.; Barnett, J. B.; Li, B. *Nanotechnol., Sci. Appl.* **2009**, *2*, 21–27.
(8) Lynn, D. M. *Adv. Mater. (Weinheim, Ger.)* **2007**, *19*, 4118–4130.
(9) Jewell, C. M.; Lynn, D. M. *Adv. Drug Delivery Rev.* **2008**, *60*, 979–999.
(10) Lu, Z.; Prouty, M. D.; Guo, Z.; Golub, V. O.; Kumar, C. S. S. R.; Lvov, Y. M. *Langmuir* **2005**, *21*, 2042–2050.
(11) Hu, S.-H.; Tsai, C.-H.; Liao, C.-F.; Liu, D.-M.; Chen, S.-Y. *Langmuir* **2008**, *24*, 11811–11818.
(12) Shchukin, D. G.; Gorin, D. A.; Möhwald, H. *Langmuir* **2006**, *22*, 7400–7404.
(13) De Geest, B. G.; Skirtach, A.; Mamedov, A.; Antipov, A.; Kotov, N.; De Smedt, S.; Sukhorukov, G. B. *Small* **2007**, *3*, 804–808.
(14) Wood, K. C.; Zacharia, N. S.; Schmidt, D. J.; Wrightman, S. N.; Andaya, B. J.; Hammond, P. T. *Proc. Natl. Acad. Sci. U.S.A.* **2008**, *105*, 2280–2285.
(15) Boulmedais, F.; Tang, C. S.; Keller, B.; Vörös, J. *Adv. Funct. Mater.* **2006**, *16*, 63–70.
(16) Recksiedler, C. L.; Deore, B. A.; Freund, M. S. *Langmuir* **2006**, *22*, 2811–2815.
(17) Wang, F.; Liu, X.; Li, G.; Li, D.; Dong, S. *J. Mater. Chem.* **2009**, *19*, 286–291.
(18) Dieguez, L.; Darwish, N.; Graf, N.; Voros, J.; Zambelli, T. *Soft Matter* **2009**, *5*, 2415–2421.
(19) Angelatos, A. S.; Radt, B.; Caruso, F. *J. Phys. Chem. B* **2005**, *109*, 3071–3076.
(20) Radt, B.; Smith, T.; Caruso, F. *Adv. Mater. (Weinheim, Ger.)* **2004**, *16*, 2184–2189.
(21) Skirtach, A. G.; Antipov, A. A.; Shchukin, D. G.; Sukhorukov, G. B. *Langmuir* **2004**, *20*, 6988–6992.
(22) Kwon, I. C.; Bae, Y. H.; Kim, S. W. *J. Controlled Release* **1994**, *30*, 155–159.
(23) Yamauchi, F.; Kato, K.; Iwata, H. *Langmuir* **2005**, *21*, 8360–8367.
(24) Choi, J.-W.; Lim, I. H.; Kim, H. H.; Min, J.; Lee, W. H. *Biosens. Bioelectron.* **2001**, *16*, 141–146.
(25) Guillaume-Gentil, O.; Akiyama, Y.; Schuler, M.; Tang, C.; Textor, M.; Yamato, M.; Okano, T.; Vörös, J. *Adv. Mater. (Weinheim, Ger.)* **2008**, *20*, 560–565.
(26) Guillaume-Gentil, O.; Graf, N.; Boulmedais, F.; Schaaf, P.; Vörös, J.; Zambelli, T. *Soft Matter* **2010**, *6*, 4246–4254.
(27) Gabi, M.; Sannomiya, T.; Larmagnac, A.; Puttaswamy, M.; Vörös, J. *Integr. Biol.* **2009**, *1*, 108–115.
(28) Picart, C.; Lavalle, P.; Hubert, P.; Cuisinier, F. J. G.; Decher, G.; Schaaf, P.; Voegel, J. C. *Langmuir* **2001**, *17*, 7414–7424.
(29) Picart, C.; Mutterer, J.; Richert, L.; Luo, Y.; Prestwich, G. D.; Schaaf, P.; Voegel, J. C.; Lavalle, P. *Proc. Natl. Acad. Sci. U. S. A.* **2002**, *99*, 12531–12535.
(30) Kwon, I. C.; Bae, Y. H.; Okano, T.; Kim, S. W. *J. Controlled Release* **1991**, *17*, 149–153.
(31) Grabarek, Z.; Gergely, J. *Anal. Biochem.* **1990**, *185*, 131–135.
(32) Richert, L.; Boulmedais, F.; Lavalle, P.; Mutterer, J.; Ferreux, E.; Decher, G.; Schaaf, P.; Noegel, J. C.; Picart, C. *Biomacromolecules* **2004**, *5*, 284.
(33) Schuetz, P.; Caruso, F. *Adv. Funct. Mater.* **2003**, *13*, 929–937.
(34) Boudou, T.; Crouzier, T.; Auzély-Velty, R.; Glinel, K.; Picart, C. *Langmuir* **2009**, *25*, 13809–13819.
(35) Richert, L.; Engler, A. J.; Discher, D. E.; Picart, C. *Biomacromolecules* **2004**, *5*, 1908–1916.
(36) Francius, G.; Hemmerlé, J.; Ohayon, J.; Schaaf, P.; Voegel, J.-C.; Picart, C.; Senger, B. *Microsc. Res. Tech.* **2006**, *69*, 84–92.
(37) Schneider, A.; Francius, G.; Obeid, R.; Schwinté, P.; Hemmerlé, J.; Frisch, B.; Schaaf, P.; Voegel, J.-C.; Senger, B.; Picart, C. *Langmuir* **2005**, *22*, 1193–1200.
(38) Schneider, A.; Richert, L.; Francius, G.; Voegel, J.-C.; Picart, C. *Biomedical Materials* **2007**, *2*, S45.
(39) Ren, K.; Crouzier, T.; Roy, C.; Picart, C. *Adv. Funct. Mater.* **2008**, *18*, 1378–1389.
(40) Semenov, O. V.; Malek, A.; Bittermann, A. G.; Vörös, J.; Zisch, A. H. *Tissue Eng., Part A* **2009**, *15*, 2977–2990.
(41) Richert, L.; Arntz, Y.; Schaaf, P.; Voegel, J.-C.; Picart, C. *Surf. Sci.* **2004**, *570*, 13–29.
(42) Buron, C. C.; Filiâtre, C.; Membrey, F.; Bainier, C.; Charraut, D.; Foissy, A. *Colloids Surf., A* **2007**, *305*, 105–111.
(43) Porcel, C.; Lavalle, P.; Decher, G.; Senger, B.; Voegel, J. C.; Schaaf, P. *Langmuir* **2007**, *23*, 1898–1904.
(44) Dubas, S. T.; Schlenoff, J. B. *Macromolecules* **1999**, *32*, 8153–8160.
(45) Halthur, T. J.; Elofsson, U. M. *Langmuir* **2004**, *20*, 1739–1745.
(46) Lvov, Y.; Haas, H.; Decher, G.; Moehwald, H.; Kalachev, A. *J. Phys. Chem.* **1993**, *97*, 12835–12841.
(47) Yoo, D.; Shiratori, S. S.; Rubner, M. F. *Macromolecules* **1998**, *31*, 4309–4318.
(48) Shiratori, S. S.; Rubner, M. F. *Macromolecules* **2000**, *33*, 4213–4219.
(49) Burke, S. E.; Barrett, C. J. *Biomacromolecules* **2003**, *4*, 1773–1783.
(50) Ren, K.; Wang, Y.; Ji, J.; Lin, Q.; Shen, J. *Colloids Surf., B* **2005**, *46*, 63–69.
(51) Wong, J. E.; Zastrow, H.; Jaeger, W.; von Klitzing, R. *Langmuir* **2009**, *25*, 14061–14070.
(52) Salomaki, M.; Vinokurov, I. A.; Kankare, J. *Langmuir* **2005**, *21*, 11232–11240.
(53) Marx, K. A. *Biomacromolecules* **2003**, *4*, 1099–1120.
(54) Kurrat, R.; Textor, M.; Ramsden, J. J.; Boni, P.; Spencer, N. D. *Rev. Sci. Instrum.* **1997**, *68*, 2172–2176.
(55) Picart, C.; Gergely, C.; Arntz, Y.; Voegel, J.-C.; Schaaf, P.; Cuisinier, F. J. G.; Senger, B. *Biosens. Bioelectron.* **2004**, *20*, 553–561.
(56) Johannsmann, D.; Reviakine, I.; Rojas, E.; Gallego, M. *Anal. Chem.* **2008**, *80*, 8891–8899.
(57) Tellechea, E.; Johannsmann, D.; Steinmetz, N. F.; Richter, R. P.; Reviakine, I. *Langmuir* **2009**, *25*, 5177–5184.
(58) Johannsmann, D.; Reviakine, I.; Richter, R. P. *Anal. Chem.* **2009**, *81*, 8167–8176.
(59) Rojas, E.; Gallego, M.; Reviakine, I. *Anal. Chem.* **2008**, *80*, 8982–8990.
(60) DeLongchamp, D. M.; Hammond, P. T. *Adv. Funct. Mater.* **2004**, *14*, 224–232.
(61) Sato, K.; Kodama, D.; Naka, Y.; Anzai, J.-i. *Biomacromolecules* **2006**, *7*, 3302–3305.
(62) Wang, F.; Li, D.; Li, G.; Liu, X.; Dong, S. *Biomacromolecules* **2008**, *9*, 2645–2652.

AM1007062